Geophys. J. Int. (2006) **166,** 814–824 doi: 10.1111/j.1365-246X.2006.03052.x

A N–S receiver function profile across the Variscides and Caledonides in SW Ireland

Michael Landes,[1] J. R. R. Ritter,[1] B. M. O'Reilly,[2] P. W. Readman[2] and V. C. Do[2]

[1]*Geophysical Institute, University of Karlsruhe, Hertzstrasse* 16, 76187 *Karlsruhe, Germany. E-mail: Michael.Landes@gpi.uni-karlsruhe.de*
[2]*Dublin Institute for Advanced Studies,* 5 *Merrion Square, Dublin* 2, *Ireland*

Accepted 2006 April 25. Received 2006 April 7; in original form 2005 May 31

SUMMARY

Teleseismic receiver functions have been calculated from data of a temporary seismological network of broad-band three-component stations to investigate the lithospheric and asthenospheric structure across the Late Caledonian Iapetus Suture Zone (ISZ) in southern Ireland. The stations were deployed during the Irish Seismological Lithospheric Experiment (ISLE 2002/3) and straddle the Killarney-Mallow Fault Zone, a remnant of the Variscan orogeny, and the ISZ, the inferred boundary between the Laurentia and Eastern Avalonia plates fused together during the Caledonian orogeny.

Receiver functions from the western part of the network were projected onto the N–S VARNET 1996 seismic refraction profile, extending from the Old Head of Kinsale to Galway Bay in SW Ireland. Laterally continuous *P* to *S* conversions from the Moho at delay times of about 3.8–4.1 s are clearly observed, and correspond to Moho depths of about 29–32 km. The Moho has a transitional character to the south of the ISZ. Synthetic receiver functions, calculated from a 2-D velocity model of the previous VARNET experiment, show Moho conversions and multiple crustal phases compatible to those observed in the ISLE data. Furthermore, *P* to *S* conversions from the 660 km discontinuity (66–68 s delay time) are well determined at the stations. In comparison, the conversion from the 410 km discontinuity at about 43–45 s delay time is considerably weaker. Delay times of stacked receiver functions from the mantle transition zone are in agreement with the standard iasp91 earth model and thus no structural changes are observed across the ISZ at this depth interval.

Key words: Caledonian orogeny, Iapetus Suture Zone, Ireland.

1 INTRODUCTION AND GEOLOGICAL BACKGROUND

The dominant trend of the structural geology throughout Ireland is northeast–southwest, as observed from surface topography and gravity mapping (Readman *et al.* 1997). This trend was developed during the closure of the Iapetus Ocean in the Late Ordovician and Early Silurian. By the end of the Silurian period, the existence of the ocean was drawing to an end. The oblique collision of the microcontinents bordering the Iapetus Ocean—Laurentia in the northwest and Eastern Avalonia in the southeast—formed a mountain chain, the Caledonian orogenic belt (Woodcock & Strachan 2000). The resulting Iapetus Suture Zone (ISZ; Phillips *et al.* 1976; Soper & Hutton 1984; Todd *et al.* 1991) extends with a NE–SW direction (grey band in Fig. 1) roughly from the present-day Shannon estuary on the west coast of Ireland across the Irish Midlands. The ISZ separates Lower Palaeozoic rocks with different stratigraphies, palaeontology, sedimentology and rocks with different tectonic structures. On the northern side of the suture deformation intensifies southwards towards the collision zone, while rocks on its southern side show a more simple style of deformation (Woodcock & Strachan 2000). The suture zone cannot generally be examined directly in Ireland, as it is covered by thick Carboniferous sedimentary rocks of the Irish Midlands. Its geophysical trace, however, has been mapped offshore Ireland, for example, due west of the Shannon estuary, by deep-seismic reflection data from the BIRPS group (Klemperer 1989; Klemperer & Hobbs 1991).

Onshore southern Ireland, three seismic refraction profiles have been deployed both along and across the ISZ (ICSSP, COOLE and VARNET in Fig. 1; Landes *et al.* 2005, for details see Jacob *et al.* 1985; Lowe & Jacob 1989; Landes *et al.* 2000). These active-source experiments provided detailed crustal and some upper-mantle *P*-wave velocity structure. Landes *et al.* (2000) associated Caledonian deformation with a 60 km wide mid-crustal zone of increased thickness beneath the Shannon estuary and also with a shallowing of the Moho discontinuity (i.e. thinning of the lower crust) and higher upper-mantle seismic velocities (Fig. 2). This suggests the presence of crustal and mantle blocks of different compositions on both sides

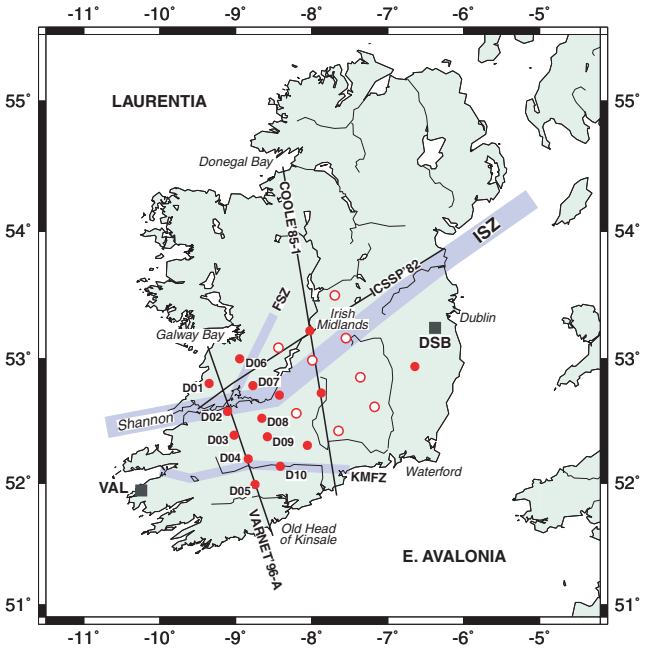

Figure 1. Map of Ireland with temporary and permanent seismic networks. Open circles: Short period instruments (three-comp), filled circles: broad-band instruments (three-comp), triangles and squares: permanent stations (one- and three-comp); DSB station is part of GEOFON network (GFZ Potsdam), VAL is operated by MET EIREANN (both three-comp). Seismic refraction profiles ICSSP (Jacob *et al.* 1985), COOLE (Lowe & Jacob 1989) and VARNET (Landes *et al.* 2000) are indicated. Also shown are the proposed location of the Iapetus Suture Zone (ISZ; broad grey band), the Killarney-Mallow Fault Zone and Fergus Shear Zone (KMFZ, FSZ; thin grey bands).

of the suture zone. A similar mid-crustal deformation zone was reported by Lowe & Jacob (1989) from the results of the COOLE seismic refraction profile (Fig. 1).

The significance of the ISZ was further revealed by a large anomaly in *P*-wave traveltime residuals derived from several teleseismic events and a Chinese nuclear explosion recorded during the VARNET controlled source experiment in 1996 (Masson *et al.* 1999; Fig. 2a). However, the crustal model of Landes *et al.* (2000) can explain only a fraction of the traveltime anomaly, which implies that considerable structural differences across the suture zone are present at subcrustal levels. Masson *et al.* (1999), therefore, modelled a steeply south-dipping boundary within the mantle lithosphere between 30 and 106 km depth, separating the two continental blocks of Laurentia and Eastern Avalonia with different seismic velocities.

In this paper we discuss the lateral variations of receiver functions across the ISZ. The receiver function analysis, which is based on seismic phase conversions (*P* to *S* and *S* to *P*), is a powerful tool in order to examine major seismic discontinuities at depth, such as the crust–mantle boundary (*P* to *S*; Zhu & Kanamori 2000), the lithosphere–asthenosphere boundary (*S* to *P*; Li *et al.* 2004), or the 410 and 660 km discontinuities (*P* to *S*; Yuan *et al.* 1997; Li *et al.* 2003). Here, we concentrate on the interpretation of *P* to *S* receiver functions.

2 ISLE TELESEISMIC DATA

The Irish Seismological Lithospheric Experiment (ISLE 2002/3, Landes *et al.* 2004) is the first teleseismic experiment conducted in Ireland and has been designed to investigate the deep lithospheric and asthenospheric structure across the Irish part of the ISZ. Between 2002 November and 2003 July, a temporary network of eight short-period instruments borrowed from the Geophysical Instrument Pool at the GeoForschungsZentrum Potsdam, Germany (open circles in Fig. 1) and 15 broad-band instruments from the Dublin Institute for Advanced Studies in Dublin, Ireland (filled circles in Fig. 1) were deployed on an almost regular grid. The aperture of the network is approximately 135 km in the NE–SW direction and 105 km in the NW–SE direction with an average spacing of about 30–50 km. Its axes were aligned approximately parallel and perpendicular to the proposed surface trace of the ISZ. The western grid lines (sites D01-D05 and D06-D10 in Fig. 1) parallel the N–S trending seismic refraction VARNET Line A (Landes *et al.* 2000). Additional data were collected from two permanent three-component broad-band stations which belong to the Irish Seismic Network and the GEOFON network (VAL and DSB, respectively, shown as squares in Fig. 1).

For this receiver function study over the western part of the network, a total of 21 teleseismic events of magnitude 6.0–7.6 from epicentral distances between 30° and 95° were used (see Table 1 and Fig. 4). Fig. 3 shows waveforms of an event on 20 June 2003 from the subduction zone underneath Brazil. The section displays vertical-component (displacement-proportional) seismograms for this magnitude 7.1 event at 558 km depth and about 80° distance. Following the *P*-wave arrival, with a signal-to-noise ratio varying between 6 and 13, a train of seismic phases (with distinct lower frequencies) including the *pP* phase that arises from the surface reflection of the upward travelling *P* wave reflected near the source and the subsequent multiple *PP* phase is seen. A similar pattern can be noticed for the *S* waves.

3 DATA PROCESSING AND RECEIVER FUNCTIONS

Data were continuously recorded in the field at either 75 or 100 sps for the broad-band stations D01-D10. After the teleseismic events were selected and the appropriate time windows extracted, the raw field data were resampled to 20 sps and converted to SeismicHandler *Q* format (Stammler 1994). Further data processing comprised the restitution of the recorded seismic signal to ground displacement. In order to restore the true ground motion, the seismometer response had to be deconvolved from the original records, that is, the data must be filtered with the inverse seismometer response function. After restitution, the data were highpass filtered (0.03 Hz) in order to remove long-wavelength filter artefacts.

Compared to most seismic stations installed on continents, the noise level observed for stations installed on islands is higher. This is especially so towards the west coast of Ireland bordering on the Atlantic Ocean. Also it is usual that a temporary network (open and filled circles in Fig. 1) will have a lower signal-to-noise ratio than a permanent network (squares in Fig. 1). In order to suppress the high to intermediate frequency noise, the data were bandpass filtered between 15 and 0.5 s (0.07–2 Hz) to highlight the Moho conversions and its multiples, and between 30 and 8 s (0.033–0.125 Hz) to highlight conversions from the mantle transition zone.

3.1 Receiver functions

Receiver functions are time-series computed from three-component seismograms. They make use of the differential times between

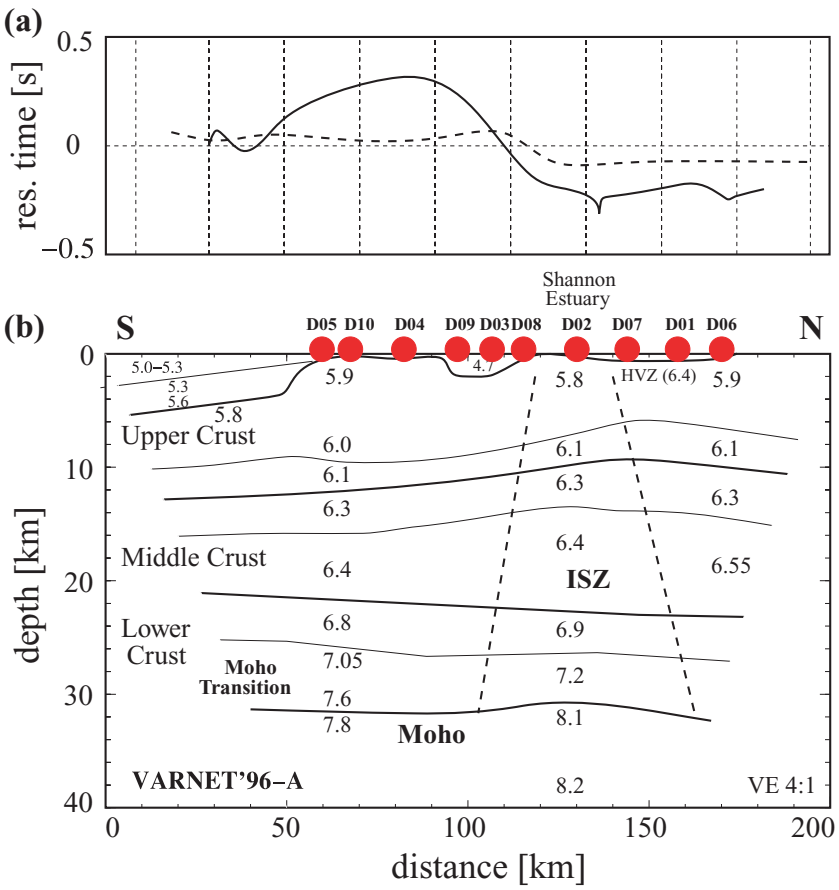

Figure 2. (a) Teleseismic traveltime residuals along VARNET Line A (modified after Masson *et al.* 1999). Continuous black line indicates observed residuals from a Chinese nuclear test, dashed line indicates calculated residuals from only using the crustal velocity model of Landes *et al.* (2000). (b) 2-D *P*-wave velocity model along the VARNET profile (modified after Landes *et al.* 2000), superimposed are locations of ISLE 2002/3 sites D01–D10.

Table 1. List of teleseismic events ranging between magnitude 6.1 and 7.8 used for receiver function analysis. Δ: Epicentral distance, AZ: Azimuth, BAZ: Backazimuth, Mw: Moment magnitude, Ms: Surface magnitude, mb: body wave magnitude after the USGS earthquake database (*http://neic.usgs.gov/neis/epic/epic.html*).

Date	UTC Time	Latitude [°]	Longitude [°]	Depth [km]	Δ [°]	AZ [°]	BAZ [°]	M	Region
2002/11/07	15:14:07	51.20	179.33	33	76.0	4.5	355.0	6.6 (Mw)	Aleutian Islands, Alaska
2002/11/17	04:53:54	47.82	146.21	459	77.0	344.0	17.5	7.3 (Mw)	NW Kuril Islands, Russia
2002/11/20	21:32:31	35.41	74.51	33	58.5	315.0	72.0	6.5 (Ms)	Northwestern Kashmir
2002/11/26	00:48:15	51.47	−173.54	20	75.0	9.0	350.5	6.1 (Mw)	Aleutian Islands, Alaska
2003/01/22	02:06:35	18.77	−104.10	24	78.5	38.0	286.0	7.6 (Ms)	Offshore Colima, Mexico
2003/01/27	05:26:23	39.50	39.88	10	35.0	309.0	93.0	6.1 (Mw)	Turkey
2003/03/15	19:41:29	52.25	160.39	30	74.5	352.5	7.5	6.0 (Mw)	E. Coast Kamchatka, Russia
2003/03/17	16:36:17	51.27	177.98	33	76.0	3.5	356.0	7.0 (Mw)	Aleutian Islands, Alaska
2003/04/17	00:48:39	37.53	96.48	14	68.5	321.0	55.5	6.4 (Mw)	Qinghai, China
2003/04/24	10:56:22	48.76	154.99	43	77.5	349.5	11.5	6.1 (Mw)	Kuril Islands, Russia
2003/05/01	00:27:05	39.01	40.46	10	35.5	309.5	93.0	6.4 (Ms)	Eastern Turkey
2003/05/14	06:03:36	18.27	−58.63	41	52.5	36.0	248.5	6.6 (Ms)	North Atlantic Ocean
2003/05/26	09:24:33	38.85	141.57	68	84.5	342.0	23.5	7.0 (Mw)	East Coast Honshu, Japan
2003/06/15	19:24:33	51.55	176.92	20	75.5	3.0	357.0	6.5 (Ms)	Aleutian Islands, Alaska
2003/06/16	22:08:02	55.49	160.00	174	71.5	352.5	7.0	6.9 (Mw)	Kamchatka Peninsula, Russia
2003/06/20	06:19:39	−7.61	−71.72	558	80.5	33.5	244.0	7.1 (Mw)	Amazonas, Brazil
2003/06/23	12:12:35	51.44	176.78	20	76.0	3.0	357.0	7.0 (Ms)	Aleutian Islands, Alaska
2003/07/15	20:27:51	−2.60	68.38	10	84.0	324.0	102.5	7.6 (Ms)	Carlsberg Ridge
2003/07/15	20:36:26	−2.40	68.68	10	84.0	323.5	102.0	5.4 (mb)	Carlsberg Ridge
2003/07/25	22:13:30	38.51	140.98	6	85.0	342.0	24.0	6.1 (Mw)	Eastern Honshu, Japan
2003/07/27	06:25:33	47.17	139.24	481	76.5	340.5	22.5	6.8 (Mw)	Primor'ye, Russia

ISLE 2002/3 list of teleseismic events used for receiver function analysis.

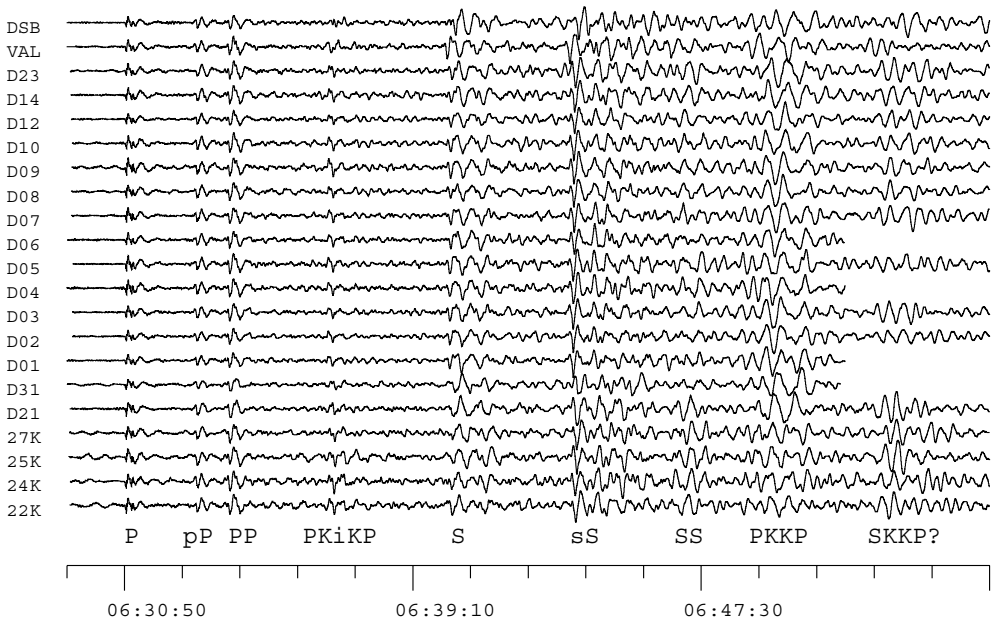

Figure 3. Vertical component waveforms of a teleseismic event beneath Brazil at 06:19:39 h on 2003 June 20 (distance 80.5°, depth 558 km, magnitude $Mw = 7.1$). The short-period data (traces 11K to 28K) have been deconvolved and simulated with a broad-band response function (30 s free period). The waveforms are aligned to the first *P*-onset time.

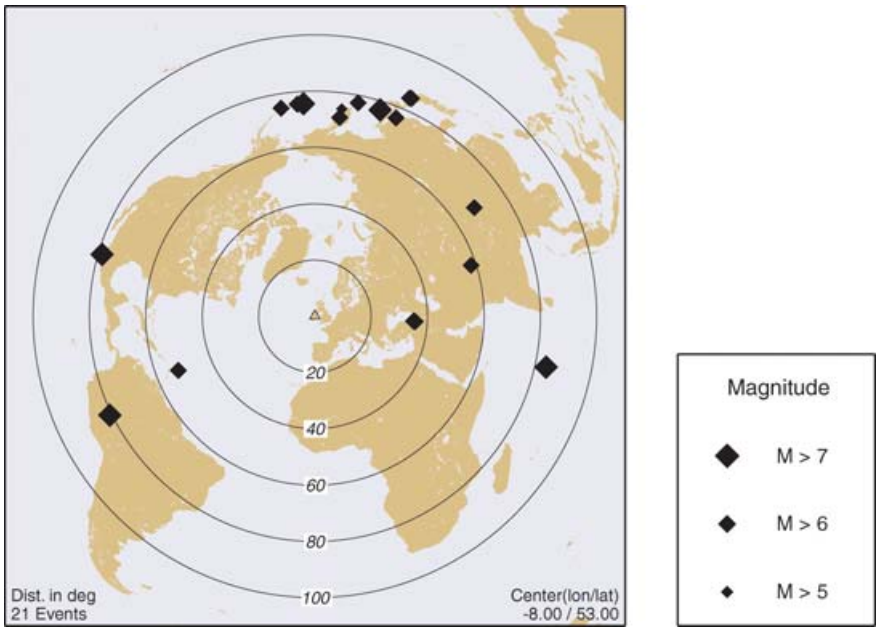

Figure 4. Azimuthal projection centred on southern Ireland showing teleseismic epicentres used in this study, recorded between 2002 November and 2003 July. Circles mark epicentral distances of 20°, 40°, 60°, 80° and 100° from southern Ireland.

transmitted *Pp* and converted *Ps* phases generated at a seismic discontinuity with a strong velocity contrast. Thus, they are a function of the medium and its conversion interfaces beneath the receiver. The *Ps* conversion reaches the receiver after the *Pp* wave, but it is often difficult to identify as it lies within the *P*-wave coda. Following Kind *et al.* (1995) and Yuan *et al.* (1997), the recorded Z, N–S and E–W traces were rotated into the LQT ray coordinate system of the incident teleseismic *P* wave (using the backazimuth and the theoretical angle of incidence). The *L* component points into the direction of the ray path and contains the *P*-wave energy, the *Q* component contains the converted *Ps* energy and is parallel to the vertically polarized *SV*-motion, and the *T* component is parallel to horizontally polarized *SH*-motion. This rotation makes it possible to fully separate *P* and *SV* wave motion which is necessary to identify converted phases and to calculate the differential times between the *Pp* and *Ps* phases. The depth of the conversion point is a function of the differential time, the *P*- and *S*-wave velocity structure below the receiver, and the *P*-wave incidence angle, or ray parameter. This depth represents an average

over an area corresponding to the first Fresnel zone. The *Ps* amplitudes depend on the velocity contrast and the angle of the incident *P* wave.

Stacking receiver functions of different events at each site suppresses random background noise and enhances the coherent conversion signal. As each seismogram includes source and propagation effects, these must be eliminated to make records from different teleseismic events comparable. Assuming that after rotation the *L* component contains the source time function, the *Q*-component is deconvolved with the *P*-wave signal on the *L* component to yield source-equalized receiver functions (Kind *et al.* 1995). Furthermore, since teleseismic waves are generated at different epicentral distances, thus arriving at the receiver with different angles of incidence and thereby causing significant traveltime delays, a distance moveout correction is necessary to align the traveltime curves of *Ps* converted phases parallel to those of the transmitted *Pp* phase. In this study, a reference distance of 67° (corresponding to a slowness of 6.4 s/°; Kind & Vinnik 1988) is used for the moveout correction.

3.2 Resolution of receiver functions

The horizontal resolution of receiver functions, that is, the area around the receiver sampled by a receiver function, depends on the radius of the first Fresnel zone of the incident *P* wave (Sheriff & Geldart 1995). For a crust–mantle boundary at 31 km depth and an upper-mantle *P*-velocity of 7.9 km s^{-1} (see Fig. 2), the radius of the corresponding Fresnel zone (assuming an incident *P* wave with a frequency of 0.3 Hz) is approximately 31 km. As a rule of thumb, the sample distance from the receiver (1/2 Fresnel radius) is approximately 1/3 of the depth to the velocity contrast of interest. The multiples (e.g. *PpPs*, *PsPs+PpSs* in Fig. 6a) average the structure over a distance about two to three times of the *Ps* conversion from the crust–mantle boundary. Because of its close sampling beneath the receiver, studying *Ps* can provide good lateral resolution of the crust–mantle boundary when a reasonable azimuthal distribution of teleseismic events is available. The vertical resolution, according to Sheriff & Geldart (1995), depends on seismic discontinuities being separated by more than 1/4 of the *S*-wave wavelength, for this study somewhere in the range of 3.5–4 km.

For the deep-mantle discontinuities at 410 and 660 km, the radius of the corresponding Fresnel zone is 160 and 200 km, respectively (Li *et al.* 2000a). If the station density is high and a large number of teleseismic events is available, then the true horizontal resolution can be determined by the area confining the conversion points.

4 LATERAL VARIATIONS OF RECEIVER FUNCTIONS ACROSS ISZ

4.1 Crustal structure

Teleseismic receiver functions have been calculated from data of 10 broad-band three-component stations (D01–D10 in Fig. 1), deployed across the Caledonian ISZ, to investigate topographic variations of the sediment-basement and crust–mantle interfaces. Site D05 lies at the edge of a 6 km thick sedimentary basin (Fig. 2) with a velocity contrast from sediment to crystalline basement of about 0.2–0.3 km s^{-1} (Landes *et al.* 2000). The basin is situated south of the Killarney-Mallow Fault Zone (KMFZ in Fig. 1), generally considered as the northern margin of Variscan deformation. Sites D10 and D04 are located in the vicinity of the fault zone, where Landes *et al.* (2000) modelled shallow upper-crustal basement overlain by a thin sedimentary layer (less than 1 km thick). The region between the KMFZ and the Shannon estuary is dominated by a 3–4 km thick sedimentary basin with a velocity contrast to crystalline basement of 1.1 km s^{-1} (sites D09 and D03). Sites D08, D02 and D07 were deployed in the vicinity of the Shannon estuary at around the proposed (surface) trace of the ISZ. The surface geology north of the suture zone, in the vicinity of sites D01 and D06, is comprised of Upper Carboniferous sediments (Sevastopulo 2001), but modelled by Landes *et al.* (2000) as a high-velocity lens (6.4 km s^{-1}) of less than 2 km thickness.

Individual and stacked receiver functions for the most northern sites D01 and D07 (see Figs 1 and 2) are presented in Fig. 5. The waveforms include the conversion from the sediment-basement discontinuity (Psed), the crust–mantle boundary (Ps), and its multiple phases that reverberate in the crust beneath the receiver (*PpPs*, *PsPs+PpSs*). The sum trace of the receiver function at D07 shows a positive peak at 1.1 s possibly indicating a *P* to *S* conversion at the base of a sedimentary layer. For a 30–32 km thick crust with a sedimentary layer of 4–6 km as shown in Fig. 2, multiple phases from the sediment-basement interface arrive between the *Psed* and the *Ps* conversions at 1–3 s delay time (Diehl 2003). Depth estimates for the sediment-basement interface, using the inversion method of Zhu & Kanamori (2000), however resulted in large discrepancies with the 2-D velocity model presented by Landes *et al.* (2000), possibly because the sediment multiples are not distinct from the *Psed* conversion.

In order to reduce the ambiguity that arises from estimating crustal thickness and v_p/v_s-ratio from only the delay time of the *Ps* conversion, the inversion method of Zhu & Kanamori (2000) searches a v_p/v_s-(Moho) depth combination that simultaneously explains *Ps* and its multiples *PpPs* and *PsPs+PpSs*. However, errors in estimating the average crustal v_p velocity will affect the computation of the Moho depth. Therefore, in order to refine the values for Moho depth, we have used average crustal velocities for each site derived from the seismic refraction model of Landes *et al.* (2000).

The sum traces of the receiver functions at sites D01 and D07 give a clear indication for a strong *Ps* conversion from the Moho at a delay time of about 3.8–4.1 s, while the multiple phases arrive at approximately 12–13 s and 16.5–17 s. Moho depths for these two sites were computed to 30.0 and 31.5 km based on average crustal velocities of 6.5 km s^{-1} and 6.43 km s^{-1} (Table 2), respectively. The corresponding v_p/v_s-ratios for D01 and D06 (1.83 and 1.8) are different from that of D07 (1.74). One possible, but speculative explanation of this v_p/v_s-variation is that the two sites are separated geologically by the NNE–SSW trending Fergus Shear Zone (FSZ in Fig. 1), which marks the western boundary of the central Ireland Variscan regime (Coller 1984). The tectonic units of the West Clare block to the west of the shear zone appear to be more deformed than to the east of it. A deeper, possibly upper-crustal, expression of the FSZ is suggested by a strong aeromagnetic lineament along its northern mapped limit, and a steep gravity gradient along its southern extent (Coller 1984).

In order to investigate lateral topographic variations of major crustal and mantle discontinuities across the ISZ, a profile was constructed by projecting the receiver functions for sites D01–D10 perpendicularly onto the VARNET profile that extended from the Old Head of Kinsale to Galway Bay (for location see Fig. 1). The result is shown in Fig. 6(a) where summed traces are normalized with respect to the maximum amplitude of each trace. The data quality of crustal receiver functions for sites D03 and D08 was inconclusive at high frequencies (0.07–2 Hz), which are therefore not presented

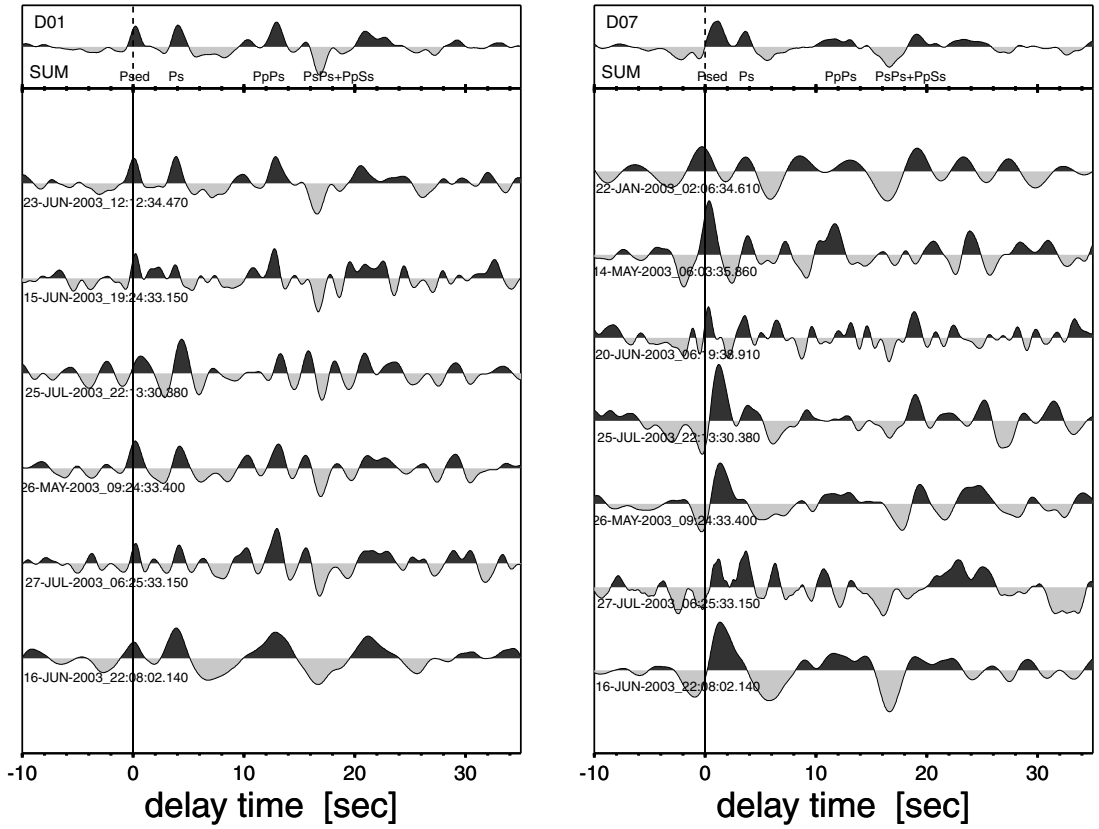

Figure 5. Receiver functions for sites D01 and D07. The top trace is the summed receiver function with clear conversions from the base of the sedimentary layer (*Psed*) and the Moho (*Ps*; multiples *PpPs*, *PsPs* + *PpSs*).

Table 2. Average crustal v_p velocities and Moho depths derived from the VARNET Line A 2-D model in Fig. 2 (Landes *et al.* 2000). Also shown, results for v_p/v_s-ratios and Moho depths calculated from receiver functions in this study. Uncertainties derived from Fig. 7 are ± 0.03 and ± 1 km.

Site	v_p [km s^{-1}]	Moho [km]	RF v_p/v_s	RF Moho [km]
D01	6.50	32.0	1.83	30.0
D02	6.40	31.0	1.72	30.5
D04	6.43	32.0	1.76	32.0
D05	6.28	31.5	1.78	29.5
D06	6.43	30.0	1.80	29.5
D07	6.43	30.0	1.74	30.5
D09	6.38	32.0	1.73	32.0
D10	6.43	31.5	1.80	32.5

Average v_p velocities and Moho depths derived from the VARNET Line A 2-D model in Fig. 2, and results from receiver functions.

in Figs 6 and 9(a). The number of receiver function traces for each site varies between 6 and 9.

The profile in Fig. 6 reveals that the receiver functions to the south of the Shannon estuary (i.e. sites D05, D10, D04 and D09) are characterized by an intracrustal conversion at delay times of 1.5–2 s (see dashed line in Fig. 6a; its significance is discussed below). A *Ps* conversion at 3.8–4.1 s is observed for all stations but is less prominent for stations to the south than to the north. Delay times for the *Ps* conversion in this study are compatible to investigations by Tomlinson *et al.* (2003) across the ISZ in Great Britain. Beneath the Shannon and to the north of it (sites D02, D07, D01 and D06), the crust is more simple with a sharp Moho phase but devoid of any intracrustal conversions. This is in agreement with results of the earlier VARNET Line A model (Fig. 2), which comprises a Moho transition zone to the south of the Iapetus suture (Shannon estuary), while beneath the Shannon and to the north of it the Moho is a first order discontinuity. Clear Moho multiples (*PpPs*, *PsPs*+*PpSs*) can be observed at 13–14 s and 16–17.5 s delay time, respectively, except for sites D05 and D10.

Moho depths along the profile, using the inversion method after Zhu & Kanamori (2000) and average crustal velocities of 6.28–6.5 km s^{-1} at individual sites (derived from the VARNET Line A model; see Table 2), vary between 29.5 and 32.5 km with a slight topographical Moho high beneath the Shannon estuary. Corresponding average crustal v_p/v_s-ratios range from 1.72 to 1.83 (Table 2, Fig. 7). We estimate the uncertainties in Moho depths and v_p/v_s-ratios from the dimensions of the 95 per cent confidence areas (white ellipse around maximum) in Fig. 7 to ± 1 km and ± 0.03, respectively. This is similar to uncertainties derived from varying the average crustal velocity by ± 0.2 km s^{-1}. The above results fit the Moho topography along VARNET Line A reasonably well within the estimated errors.

A synthetic receiver function profile was generated along VARNET Line A (Fig. 6 b). The input models were derived by digitizing the 2-D velocity model (Fig. 2) into a series of individual 1-D velocity-depth functions. Then, a plane wave approximation, based on the reflectivity algorithm described by Müller (1985), was used to compute the receiver function response of a stack of homogeneous, isotropic layers above a half-space. The calculated average crustal v_p/v_s-ratios for sites D01–D10 were used as *a priori* information. Examination of the synthetic receiver functions in Fig. 6(b)

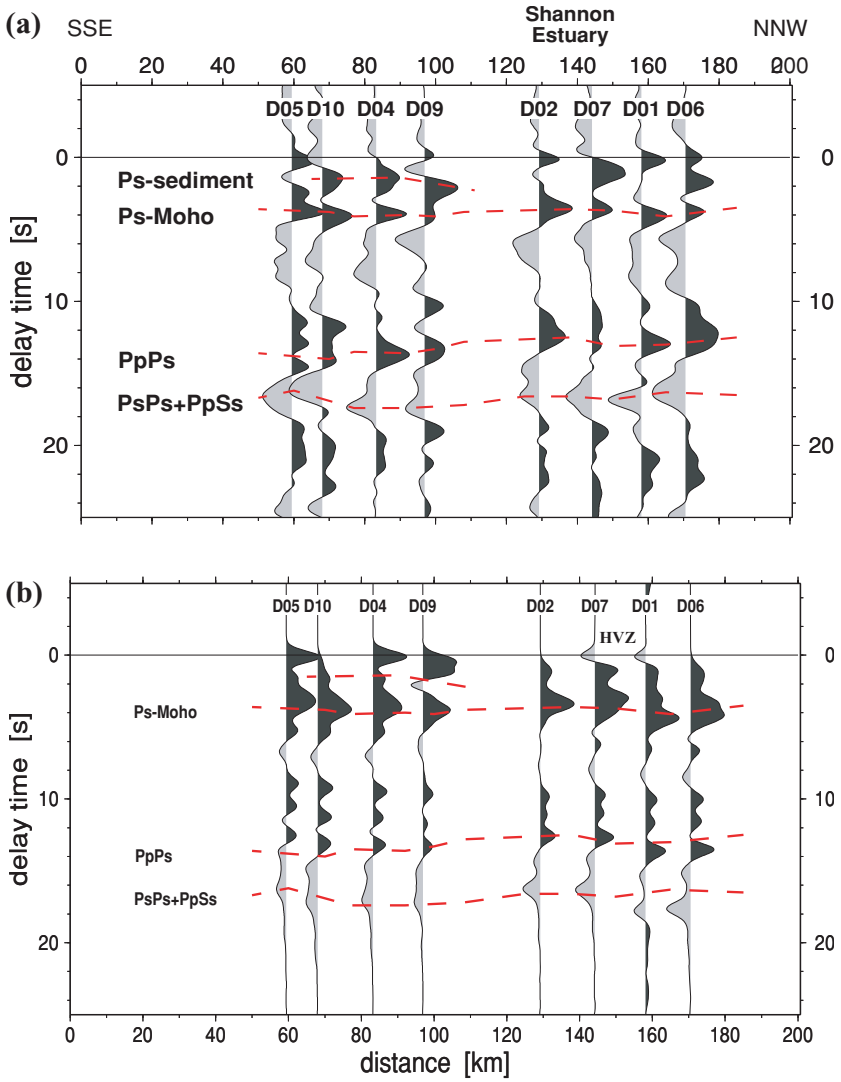

Figure 6. (a) Moveout-corrected summed receiver functions for sites D01–D10 along VARNET Line A. The timescale resembles the delay times of *P* to *S* converted (and multiple) phases relative to the *P* arrival time at 0 s. Positive amplitudes are shaded black, meaning conversions at a sudden velocity increase with depth. (b) Synthetic receiver functions derived from the 2-D velocity model in Fig. 2(b) at individual receiver sites.

shows Moho conversions and multiple crustal phases compatible to those derived from the observed ISLE data. However, there is a discrepancy in delay time between the synthetic and observed receiver functions (at about 4 s) to the south of the Shannon estuary. The earlier arrival times of the synthetic *Ps* phase (based on the seismic refraction model) may be caused by either (1) decreasing crustal thickness, (2) increasing average crustal v_p velocity or (3) decreasing crustal v_p/v_s-ratio. Alternatively, this phase is more likely to resemble the conversion from the top of the lower crust, while the smaller peaks at about 2 s (dashed line in Fig. 6b) are due to the conversion at the mid-crustal interface. Thus, the broadening of the observed pulse is attributed to the interference of the intracrustal and Moho conversions.

The synthetic receiver functions for sites D01 and D07 exhibit a negative amplitude (see label HVZ in Fig. 6b), indicative of a conversion at a velocity contrast with downward decreasing velocities, that results from the near-surface high-velocity zone north of the Shannon estuary, as modelled by Landes *et al.* (2000). This is not confirmed by the observed receiver functions at sites D01 and D07 (Figs 5 and 6a). Its presence, although based on very high apparent velocities in the seismic refraction data, therefore, remains speculative.

4.2 Mantle transition zone

Although it is not expected that the effect of an oblique continent-continent collision zone such as in Ireland still extends as deep as the mantle transition zone (410–660 km depth), the data quality has allowed examination of *P* to *S* conversions from discontinuities at these depths. For that purpose, data from sites D01–D10 were bandpass filtered between 30 and 8 s to highlight the lower frequency (long-wavelength) conversion arrivals from the 410 and 660 km discontinuities. It should be noted that the signal-to-noise ratio of the deep mantle conversions was clearly improved when the cut-off period of the bandpass filter was shifted to periods above 30 s, but to the expense of spatial resolution.

Stacked receiver functions for sites D01–D10 (Fig. 8a) show *P* to *S* conversions from the mantle transition zone in a delay time window between 30 and 80 s. Theoretical traveltimes of the 410

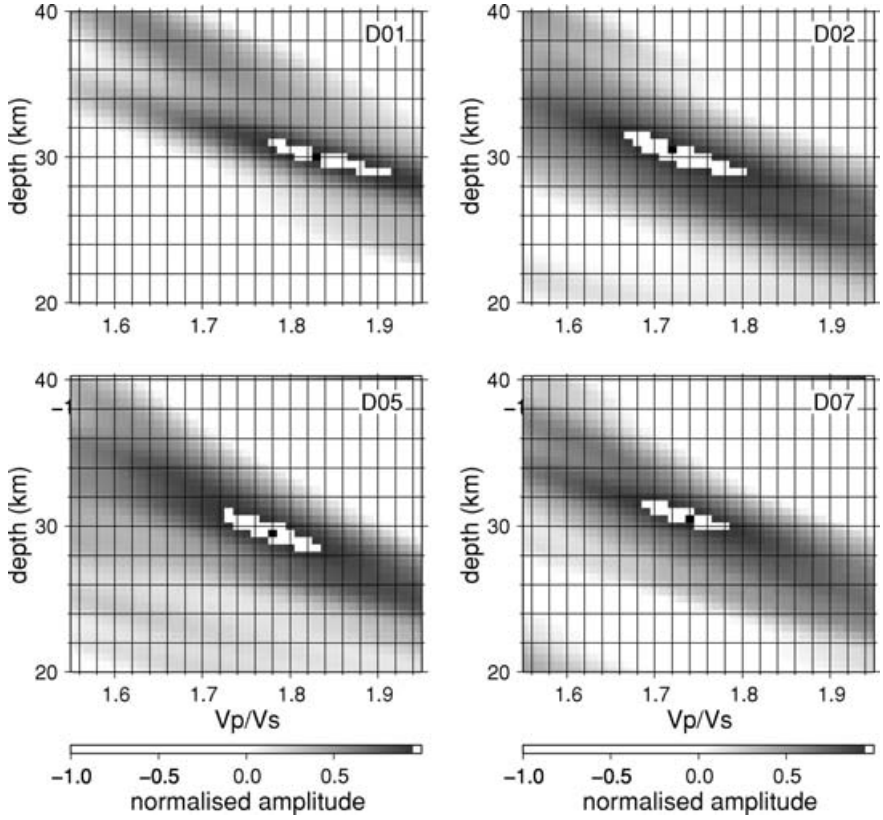

Figure 7. Moho depths and v_p/v_s-ratios (black rectangle within white ellipse representing 95 per cent confidence level) for sites D01, D02, D05 and D07 using the inversion method of Zhu & Kanamori (2000).

and 660 km phases for the standard iasp91 earth model (Kennett & Engdahl 1991) are 44 and 68 s, calculated for a reference distance of 67°. A weak phase at about 43–45 s might be associated with the conversion from the 410 km mantle discontinuity (P410s). Below that, the more prominent phase between 64 and 69 s, seen in all receiver function traces, is associated with the 660 km discontinuity (P660s). The large variations in delay times of the P410s and P660s phases could be caused by low signal-to-noise ratios of individual receiver function traces. However, it must be remembered that the P410s and P660s conversion points (Fig. 8b) are located far away from the individual receiver sites, for example, for an event at 67° epicentral distance they are offset by 118 and 216 km, respectively, (Li *et al.* 2000a). We, therefore, stacked the receiver functions for similar P410s and P660s conversion points (P410s: 18–43 traces, P660s: 6–13 traces; see boxes in Fig. 8b). In Fig. 8(c), there is no significant difference in delay times for the two phases across the suture. Uncertainties in delay times for the stacked P410s and P660s conversions amount to ±2.5–3.5 s and ±1.5–2.0 s, with respect to the theoretical values. Furthermore, delay times for the two phases both north and south of the ISZ agree well with those computed from the iasp91 model (thin lines in Fig. 8c). The P660s–P410s differential times for the stacked receiver functions differ by less than 0.5 s from the theoretical value of 24 s.

We observe an amplitude ratio between P660s and P410s of 2–4, which is compatible to the iasp91 model (Budweg 2002) but significantly higher compared to other studies which often report P660s/P410s amplitude ratios of 1 or less (Yuan *et al.* 1997; Bostock 1998; Kosarev *et al.* 1999; Li 2000; Li *et al.* 2000b; Ramesh *et al.* 2002). Benz & Vidale (1993), in agreement with Petersen *et al.* (1993), modelled the 410 km discontinuity as a velocity gradient zone of 4–6 km thickness which significantly shifted the amplitude ratio in favour of the 660 km discontinuity. The weak P410s conversion may suggest an unusually small, but sharp velocity contrast, a velocity gradient zone, or a combination of both across the top of the mantle transition zone beneath Ireland.

4.3 Migration to depth

Migration allows the transformation of the receiver functions from the time into the depth domain (Grunewald *et al.* 2001). The incoming teleseismic waves are traced back through a reference velocity model, starting with the known angles of incidence and backazimuth. For this study, the reference model was divided into volume elements of $5 \times 5 \times 5$ km^3. For each site, the crustal velocity model along VARNET Line A (Fig. 2; Landes *et al.* 2000) replaced the top layers of the global iasp91 model of Kennett & Engdahl (1991). The amplitudes of each receiver function are assumed to be caused by conversions at discontinuities within these volume elements. The contributions to each element are stacked in order to reduce noise. We then projected these volume elements onto the VARNET profile (Fig. 1). The image strongly depends on the number and azimuthal distribution of the teleseismic events.

Fig. 9 displays the migrated receiver function profile for sites D01–D10. Positive conversion amplitudes, caused by discontinuities with downward increasing velocities, are shaded red. Superimposed on Fig. 9(a) are the main intracrustal interfaces extracted from the VARNET model (see Fig. 2). The (migrated) Moho is a continuous, though blurred, feature that lies somewhere between 25 and 35 km depth, roughly coinciding with the Moho determined from

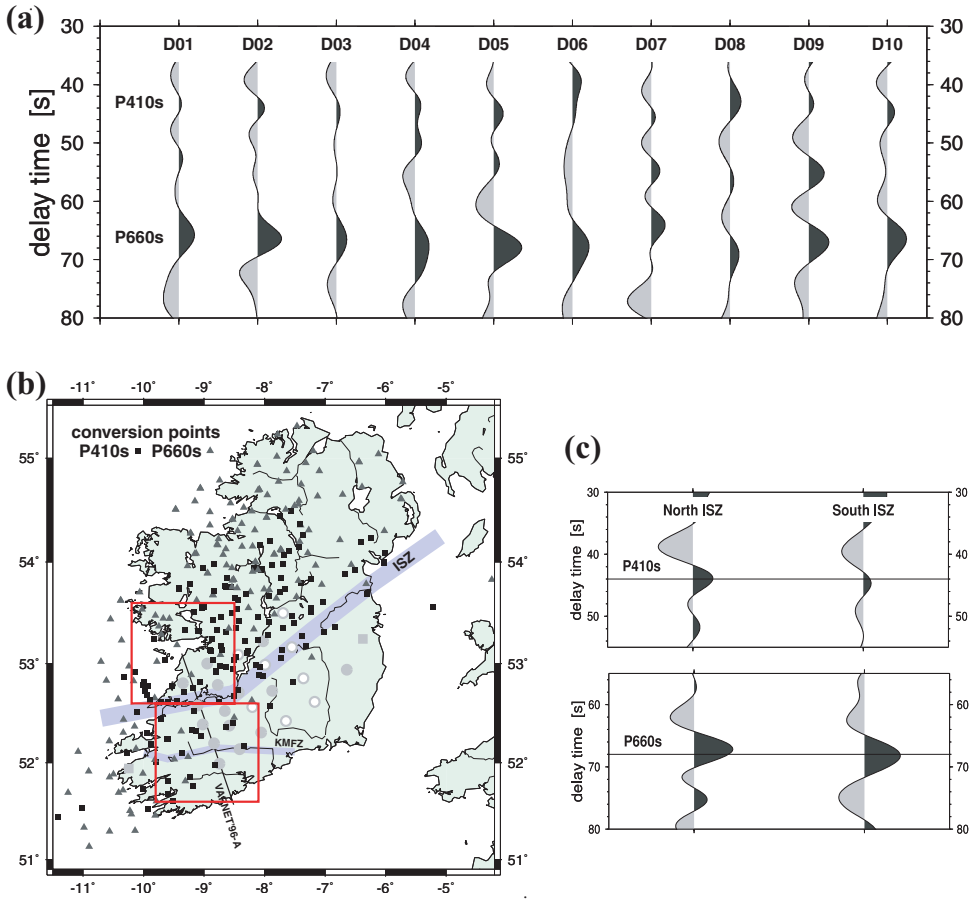

Figure 8. (a) Receiver functions for sites D01–D10 displaying conversions at the mantle transition zone (P410s, P660s) between 30 and 80 s delay time. (b) Conversions points (P410s, P660s) at the 410 and 660 km discontinuities, and (c) receiver functions stacked within the area outlined by the boxes north and south of the Shannon estuary in the vicinity of VARNET Line A.

seismic refraction data. Additionally, Moho depths, derived from the receiver functions with the method of Zhu & Kanamori (2000), are plotted with a dot size indicating the uncertainty in depth (estimated from varying the average crustal velocity by ± 0.2 km s^{-1}). The intracrustal interfaces are less well resolved, possibly because of the smaller velocity contrasts across them.

In Fig. 9(b) the migrated receiver functions are shown in the depth range of 250–800 km. The P660s conversion from the bottom of the mantle transition zone, marked by a thin straight line according to the delay time of the iasp91 reference model (Kennett & Engdahl 1991), is clearly identified. However, no indication for a deep-seated signature of the ISZ is observed. A spatial smoothing of 20×10 km^2 was applied to enhance the phase correlation of the upper mantle discontinuities. In spite of this, the P410s conversion is not seen as a continuous feature. Furthermore, receiver function phases at 320, 520–560 and below 660 km are possibly multiples from the Moho or sediments as shown with synthetics by Budweg (2002).

5 CONCLUSIONS

The receiver functions show only minor structural changes across the ISZ for the crust–mantle boundary. This might be a result of post-Caledonian tectonic movements. The crustal thickness calculated from the receiver functions lies between 29 and 32 km with the suggestion of a topographic high beneath the Shannon estuary, compatible with the seismic refraction model along VARNET Line A (Landes *et al.* 2000). Also, synthetic receiver functions derived from the VARNET model show a broad correlation with the observed data.

Migrating the receiver function time-series to depth allowed examination of the 410 and 660 km discontinuities confining the mantle transition zone. The weak conversion from the 410 km discontinuity, compared to the P660s phase, might be explained by a small velocity contrast or a velocity gradient zone across the top of the mantle transition zone. There is also no clear indication for the deep Iapetus Suture, such as a significant variation in depth of the discontinuities in the vicinity of the Shannon estuary, thus ruling out the existence of a significant thermal anomaly at the mantle transition zone beneath Ireland.

Analysis of subcrustal discontinuities using *P* to *S* receiver functions is complicated by the presence of the two crustal multiples *PpPs* and *PsPs+PpSs* which effectively mask the time interval at which direct *Ps* phases originating at depths between 100 and 200 km would arrive. Further evaluation of the data by SKS splitting to characterize upper mantle anisotropy (Do *et al.* 2006) and the computation of *S* to *P* receiver functions will unravel the region between the crust and the mantle transition zone in order to fully explain the origin of the observed variation in traveltime residuals across the ISZ.

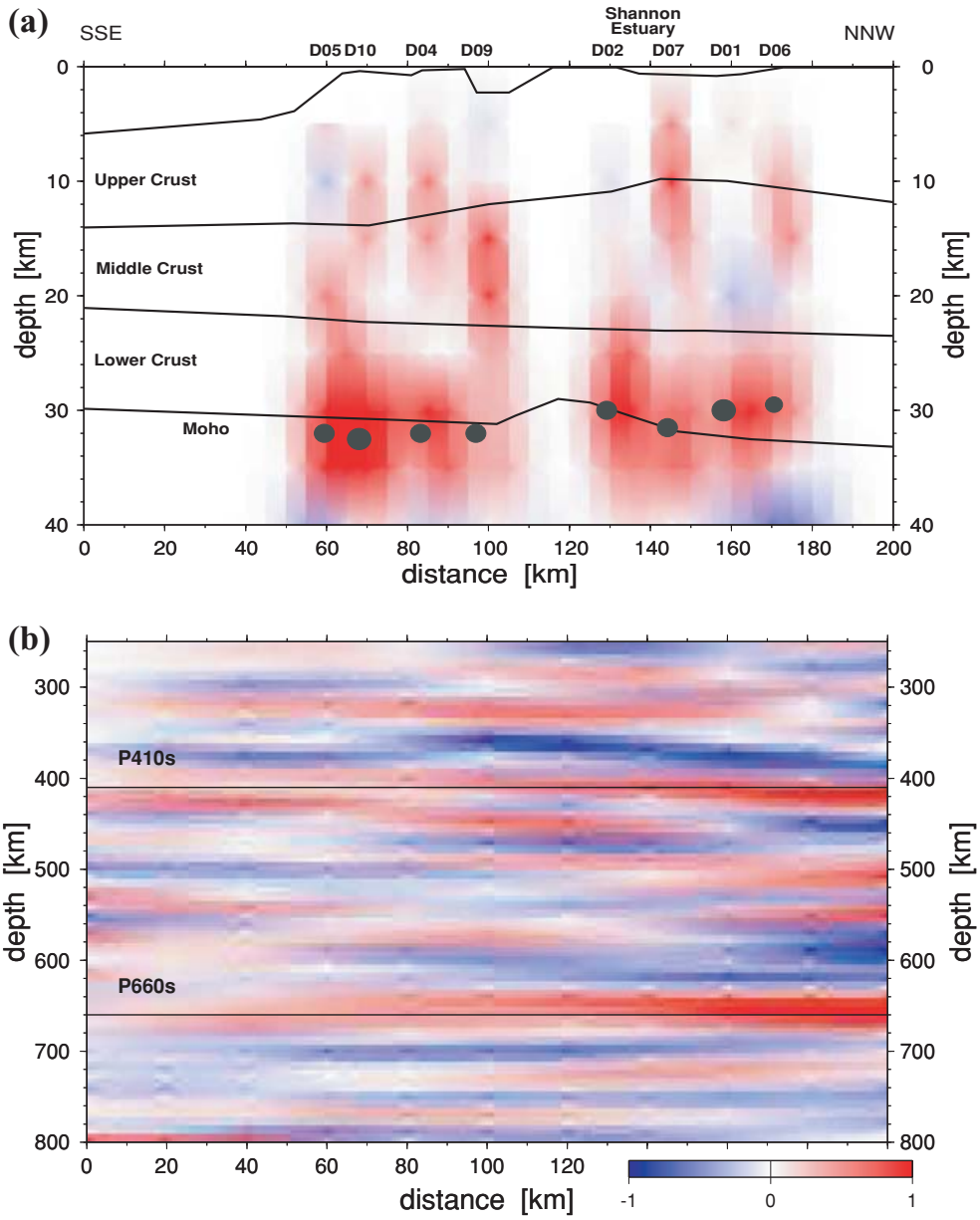

Figure 9. Migrated receiver function profile for sites D01–D10 along VARNET Line A. Positive conversion amplitudes are shaded red, see colour scale. (a) Crust: Black lines represent main interfaces derived from the 2-D velocity model in Fig. 2. Superimposed are Moho depths from receiver function study (dot size according to estimated uncertainty in depth). (b) Mantle transition zone: A spatial smoothing filter of 20 × 10 km^2 was applied. Thin lines mark the P410s and P660s conversion delay times according to the iasp91 reference model of Kennett & Engdahl (1991).

ACKNOWLEDGMENTS

ISLE 2002/3 is funded by an Enterprise Ireland Basic Research Grant (SC/2001/155) and the Deutsche Forschungsgemeinschaft, Bonn (grant Ri 1133/1). It is a collaboration between the Dublin Institute for Advances Studies (DIAS) in Ireland and the Geophysical Institute (GPI) of the University of Karlsruhe in Germany. Eight short-period mobile stations were provided by the Geophysical Instrument Pool at the GeoForschungsZentrum Potsdam, Germany. The software for computation of the synthetic receiver functions is the courtesy of J. Saul (GFZ Potsdam). Most of the data processing was performed with the SeismicHandler package from Stammler (1994). Maps and graphical display of receiver functions were plotted with the GMT software of Wessel & Smith (1995). We thank Shen and Gao for their thorough review of this paper.

REFERENCES

Benz, H.M. & Vidale, J.E., 1993. Sharpness of upper mantle discontinuities determined from high frequency reflections, *Nature,* **365,** 147–150.

Bostock, M.G., 1998. Mantle stratigraphy and evolution of the Slave province, *J. geophys. Res.,* **103,** 21 183–21 200.

Budweg, M., 2002. Der obere Mantel in der Eifel-Region untersucht mit der Receiver Function Methode. PhD thesis (University of Potsdam) and Sci. Tech. Rep. STR 03/04 (GFZ Potsdam), 117 pp.

Coller, D.W., 1984. Variscan structures in the Upper Palaeozoic rocks of west central Ireland, in *Variscan Tectonics of the North Atlantic Region,* Vol. 14, pp. 185–194, eds Hutton, D.H.W. & Sanderson, D.J., Geological Society London, Special Publication.

Diehl, T., 2003. Die Krustenstruktur Südost-Rumäniens aus der Analyse teleseismischer Receiver Funktionen, Unpublished *diploma thesis,* University of Karlsruhe, 114 pp.

Do, V.C., Readman, P.W., O'Reilly, B.M. & Landes, M., 2006. Shear-wave splitting observation across South West Ireland, *Geophys. Res. Lett.,* **33,** doi:10.1029/2005GL024496.

Grunewald, S., Weber, M. & Kind, R., 2001. The upper mantle under Central Europe: indications for the Eifel plume, *Geophys J. Int.,* **147,** 590–601.

Jacob, A.W.B., Kaminski, W., Murphy, T., Phillips, W.E.A. & Prodehl, C., 1985. A crustal model for a NE–SW profile through Ireland, *Tectonophysics,* **113,** 75–103.

Kennett, B.L.N. & Engdahl, E.R., 1991. Traveltimes for global earthquake location and phase identification, *Geophys. J. Int.,* **105,** 429–465.

Kind, R. & Vinnik, L., 1988. The upper mantle discontinuities underneath GRF array from *P* to *S* converted phases, *J. Geophys.,* **62,** 138–147.

Kind, R., Kosarev, G.L. & Petersen, N.V., 1995. receiver functions at the stations of the German Regional Seismic Network (GRSN), *Geophys. J. Int.,* **121,** 191–202.

Klemperer, S.L., 1989. Short paper: seismic reflection evidence for the location of the Iapetus suture west of Ireland, *J. geol. Soc., Lond.,* **146,** 409–412.

Klemperer, S.L. & Hobbs, R.W., 1991. *The BIRPS Atlas. Deep Seismic Reflection Profiles Around the British Isles,* Cambridge University Press, Cambridge, UK, 124 pp. and 100 seismic section.

Kosarev, G., Kind, R., Sobolev, S.V., Yuan, X., Hanka, W. & Oreshin, S., 1999. Seismic evidence for a detached Indian lithospheric mantle beneath Tibet, *Science,* **283,** 1306–1309.

Landes, M., Prodehl, C., Hauser, F., Jacob, A.W.B. & Vermeulen, N.J., 2000. VARNET-96: influence of Variscan and Caledonian orogenies on crustal structure in SW Ireland, *Geophys. J. Int.,* **140,** 660–676.

Landes, M., Ritter, J.R.R., Do, V.C., Readman, P.W. & O'Reilly, B.M., 2004. Passive teleseismic experiment explores the deep subsurface of southern Ireland, *EOS, Trans. Am. geophys. Un.,* **85**(36), 337–341.

Landes, M., Ritter, J.R.R., Readman, P.W. & O'Reilly, B.M., 2005. A review of the Irish crustal structure and its signatures from the Caledonian and Variscan orogenies, *TerraNova,* **17,** 111–120.

Li, X., 2000. A receiver function study of the northwest Pacific subduction zone and the Hawaiian mantle plume. Unpublished *PhD thesis,* University of Berlin, 122 pp.

Li, X., Sobolev, S.V., Kind, R., Yuan, X. & Estabrook, Ch., 2000a. A detailed receiver function image of the upper mantle discontinuities in the Japan subduction zone, *Earth planet. Sci. Lett.,* **183,** 527–541.

Li, X., Kind, R., Priestley, K., Sobolev, S.V., Tilmann, F., Yuan, X. & Weber, M., 2000b. Mapping the Hawaiian plume conduit with converted seismic waves, *Nature,* **405,** 938–941.

Li, X., Kind, R. & Yuan, X., 2003. Seismic study of upper mantle and transition zone beneath hotspots, *Phys. Earth planet. Int.,* **136,** 79–92.

Li, X., Kind, R., Yuan, X., Wölbern, I. & Hanka, W., 2004. Rejuvenation of the lithosphere by the Hawaiian plume, *Nature,* **427,** 827–829.

Lowe, C. & Jacob, A.W.B., 1989. A north-south seismic profile across the Caledonian Suture zone in Ireland, *Tectonophysics,* **168,** 297–318.

Masson, F., Hauser, F. & Jacob, A.W.B., 1999. The lithospheric trace of the Iapetus Suture in SW Ireland from teleseismic data, *Tectonophysics,* **302,** 83–89.

Müller, G., 1985. The reflectivity method—a tutorial, *J. Geophys.,* **58,** 153–174.

Petersen, N., Vinnik, L., Kosarev, G., Kind, R., Oreshin, S. & Stammler, K., 1993. Sharpness of mantle discontinuities, *Geophys. Res. Lett.,* **20,** 859–862.

Phillips, W.E.A., Stillman, C.J. & Murphy, T., 1976. A Caledonian plate tectonic model, *J. geol. Soc. Lond.,* **132,** 579–609.

Ramesh, D.S., Kind, R. & Yuan, X., 2002. Receiver function analysis of the North American crust and upper mantle, *Geophys. J. Int.,* **150,** 91–108.

Readman, P.W., O'Reilly, B.M. & Murphy, T., 1997. Gravity gradients and upper-crustal tectonic fabrics, Ireland, *J. geol. Soc. Lond.,* **154,** 817–828.

Scherbaum, F., 2001. *Of Poles and Zeros—Fundamentals of Digital Seismology,* 2nd edn, Kluwer Academic Publishers, Dordrecht, 268 pp.

Sevastopulo, G.D., 2001. Carboniferous (Silesian), in *The Geology of Ireland,* pp. 289–312, ed. Holland, C.H., Dunedin Academic Press, Edinburgh, 531 pp.

Sheriff, R. & Geldart, L., 1995. *Exploration Seismology,* Vol.,II. Cambridge University Press, Cambridge, 592 pp.

Soper, N.J. & Hutton, D.H.W., 1984. Late Caledonian sinistral displacements in Britain: Implications for a three-plate collision, *Tectonics,* **3,** 781–794.

Stammler, K., 1994. SeismicHandler—programmable multichannel data handler for interactive and automatic processing of seismological data, *Computers &Geosciences,* **19** (2), 135–140.

Todd, S.P., Murphy, F.C. & Kennan, P.S., 1991. On the trace of the Iapetus suture in Ireland and Britain, *J. Geol. Soc.,* **148,** 869–880.

Tomlinson, J.P., Denton, P., Maguire, P.K.H. & Evans, J.R., 2003. UK crustal structure close to the Iapetus Suture: a receiver function perspective, *Geophys. J. Int.,* **154,** 659–665.

Yuan, X., Ni, J., Kind, R., Mechie, J. & Sandvol, E., 1997. Lithospheric and upper mantle structure of southern Tibet from a seismological passive source experiment, *J. geophys Res.,* **102,** 27 491–27 500.

Wessel, P. & Smith, W.H.F., 1995. New version of the Generic Mapping Tools, *EOS, Trans. Am. geophys. Un.,* **76,** 329.

Woodcock, N.H. & Strachan, R.A., 2000. The Caledonian Orogeny: a multiple plate collision, in *Geological History of Britain and Ireland,* eds Woodcock, N.H. & Strachan, R.A., Blackwell Science, UK.

Zhu, L. & Kanamori, H., 2000. Moho depth variation in southern California from teleseismic receiver functions, *J. geophys. Res.,* **105,** 2969–2980.